THE ASTROPHYSICAL JOURNAL, 246:113–121, 1981 May 15

THE PARTIALLY IONIZED GAS IN THE W3 COMPLEX: C90α OBSERVATIONS

D. T. JAFFE
Harvard-Smithsonian Center for Astrophysics
AND
T. L. WILSON
Max-Planck-Institut für Radioastronomie
Received 1980 July 21; accepted 1980 November 19

ABSTRACT

We have mapped the distribution of the C90α line toward W3 with 90″ resolution. The emission is centered at $\alpha = 02^h21^m50\overset{s}{.}6 \pm 1\overset{s}{.}5$, $\delta = 61°52'31'' \pm 9''$ (1950), that is, southwest of W3 A (IRS 2) and toward W3 B (IRS 3). If the source and the beam are Gaussian shaped, the deconvolved source size is (121″ ± 17″, 88″ ± 15″) in (α, δ). The carbon emission covers a region which includes all of the compact radio continuum sources at the center of the W3 complex. The C II emission region shows a velocity gradient: from −39 km s^{-1} in the east to −42 km s^{-1} in the west. It is not possible to derive uniquely the electron temperature and density of the partially ionized gas from our data or from our data in conjunction with other C II results. The carbon region may consist of shells surrounding the compact H II regions.

Subject headings: nebulae: individual — radio sources: lines

I. INTRODUCTION

The W3 region contains young compact H II regions such as W3 B, the older shell-like H II region W3 A, OH and H_2O masers, and giant molecular clouds (see, e.g., Mezger and Wink 1975). Ogura and Ishida (1976) derive a photometric distance of 1.8 kpc from the OB stars in IC 1795, while the kinematic distance to W3 is 3 kpc (Reifenstein *et al.* 1970). Aperture synthesis observations of the main radio continuum emission region show that there are seven sources concentrated in a 1′×3′ area (Harris and Wynn-Williams 1976). In addition to the fully ionized and molecular clouds, this complex contains one of the most widely studied carbon recombination line regions. Carbon lines form in the partially ionized gas in complexes containing both H II regions and dense molecular clouds. They therefore serve as good tracers of the dynamics of ionization fronts in regions around OB stars (Jaffe and Pankonin 1978). Most of the carbon measurements toward W3 were made at low frequencies, where the line intensity is larger but where the telescope beams are also large. The few observations made at frequencies above 5 GHz, where the angular resolution is better, have poor signal-to-noise ratios. These data include detections of the carbon line at ∼−40 km s^{-1} only toward the continuum peak (see the compilation of observations in Rickard, Zuckerman, and Palmer 1977). Gordon and Churchwell (1970) and Chaisson (1971) reported, in addition, the existence of a weak carbon feature at −20 km s^{-1}.

We present here the results of C90α mapping carried out with the Max-Planck-Institut für Radioastronomie 100 m telescope. The great improvement in spatial resolution and sensitivity over previous measurements has permitted us to map the spatial distribution and velocity pattern of the carbon source for the first time.

II. OBSERVATIONS

We observed the He 90α and C90α lines (rest frequencies 8876.184 and 8876.995 MHz, respectively) toward W3 in 1977 September with the 100 m telescope of the Max-Planck-Institut für Radioastronomie. The full width to half-power of the telescope beam is 90″ at the rest frequency of the C90α line, and the aperture and beam efficiencies are 0.45 and 0.63 respectively. We converted all temperatures to a scale of main-beam brightness using narrow-band continuum scans of the calibration source NGC 7027. We assume this source has a flux density of 6.2 Jy at 8.9 GHz. The pointing accuracy was ±8″ rms. The receiver was a two-channel parametric amplifier. We used the channels to observe orthogonal linear polarizations. The system temperature was ∼80 K on cold sky. We took the spectra using an autocorrelator as two 192 channel spectrometers. Each spectrometer analyzed a 5 MHz bandwidth centered between the He 90α and C90α lines. At the line frequency, the velocity resolution was 1.06 km s^{-1}. We made the observations in the position-switching mode with the reference position ∼15 minutes of time west of the source.

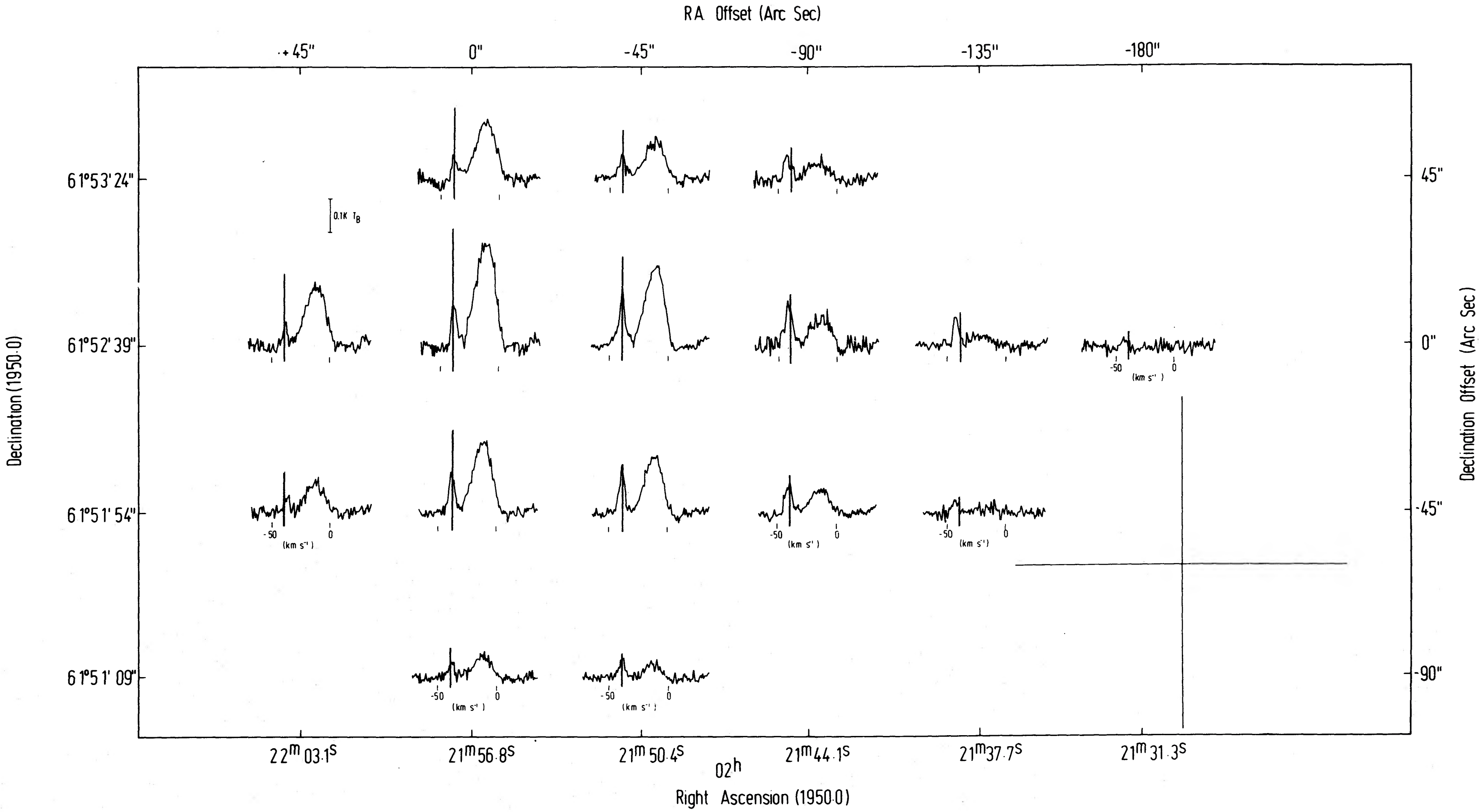

FIG. 1.—C90α and He 90α spectra toward W3. The outer box gives the coordinates in R.A. and decl. (1950) and relative to the center of W3A in arc seconds. The position of 0 and -50 km s^{-1} is marked below each spectrum, and the vertical line through each is at -40 km s^{-1}. The bar in the upper left corner gives the temperature scale, and the cross in the lower left corner represents the beam size.

TABLE 1

C90α LINE PARAMETERS

POSITION ΔR.A. (″)	POSITION ΔDecl. (″)	T_L^B (K)	V_L (km s^{-1})	ΔV_L (km s^{-1})	$T_L^B \Delta V_L$ (K km s^{-1})	RMS NOISE (K)
−180	0	0.029 (0.006)	−43.2 (0.6)	5.5 (1.5)	0.16 (0.05)	0.011
−135	−45	0.035 (0.006)	−42.8 (0.6)	6.2 (1.4)	0.22 (0.05)	0.011
−135	0	0.087 (0.006)	−43.1 (0.2)	5.2 (0.4)	0.46 (0.03)	0.010
−90	−45	0.095 (0.005)	−40.6 (0.2)	8.0 (0.5)	0.76 (0.05)	0.010
−90	0	0.113 (0.008)	−42.2 (0.3)	8.4 (0.8)	0.95 (0.10)	0.017
−90	+45	0.078 (0.006)	−42.5 (0.3)	7.5 (0.7)	0.59 (0.05)	0.011
−45	−90	0.054 (0.005)	−39.4 (0.3)	6.5 (0.7)	0.35 (0.05)	0.008
−45	−45	0.137 (0.006)	−39.4 (0.1)	6.0 (0.3)	0.81 (0.05)	0.011
−45	0	0.149 (0.006)	−39.8 (0.2)	7.8 (0.5)	1.17 (0.08)	0.013
−45	+45	0.067 (0.005)	−39.8 (0.4)	10.2 (1.0)	0.68 (0.08)	0.011
0	−90	0.046 (0.005)	−39.2 (0.4)	6.2 (0.9)	0.29 (0.05)	0.010
0	−45	0.122 (0.006)	−39.0 (0.1)	6.5 (0.4)	0.78 (0.05)	0.010
0	0	0.144 (0.010)	−38.9 (0.2)	6.4 (0.5)	0.92 (0.08)	0.017
0	+45	0.073 (0.005)	−38.4 (0.3)	9.3 (0.8)	0.67 (0.06)	0.011
+45	−45	0.049 (0.006)	−37.9 (0.4)	5.7 (1.0)	0.27 (0.05)	0.011
+45	0	0.070 (0.006)	−38.7 (0.3)	6.4 (0.8)	0.44 (0.06)	0.013
3′ Composite		0.089 (0.003)	−39.4 (0.1)	7.8 (0.4)	0.70 (0.03)	0.006

NOTE.—The errors are 1 σ formal errors from the Gaussian fits. The positions are relative to the center of W3 A (IRS 2): $\alpha(1950)=02^h21^m56^s.8$, $\delta(1950)=+61°52'35''$.

We reduced the spectra by subtracting linear baselines from the original data and adding the spectra from the two channels together. Figure 1 shows the spectra reduced using this procedure. The vertical axes give the declination and declination offset in arc seconds from the center of W3 A ($\alpha=02^h21^m56^s.8$, $\delta=61°52'39''$, 1950.0) for each of the spectra, and the horizontal axes give the right ascension and R.A. offset in arc seconds. Beneath each column of spectra we show the velocity axes with the positions of 0 and -50 km s^{-1} marked. The vertical line through each spectrum at -40 km s^{-1} serves to orient the eye. In the lower right-hand portion of the figure is a cross which indicates the full width to half-power of the telescope beam. We have removed the

TABLE 2

He 90α LINE PARAMETERS

POSITION ΔR.A. (″)	POSITION ΔDecl. (″)	T_L^B (K)	V_L (km s^{-1})	ΔV_L (km s^{-1})	$T_L^B \Delta V_L$ (K km s^{-1})
−180	0	...	...	...	...
−135	−45	...	...	...	...
−135	0	0.037 (0.005)	−49.4 (1.0)	24.2 (3.5)	0.87 (0.17)
−90	−45	0.083 (0.005)	−41.8 (0.3)	21.9 (1.3)	1.75 (0.16)
−90	0	0.092 (0.008)	−42.5 (0.5)	20.0 (2.0)	1.90 (0.32)
−90	+45	0.063 (0.005)	−44.6 (0.6)	24.4 (2.3)	1.54 (0.22)
−45	−90	0.046 (0.003)	−40.8 (0.5)	15.0 (1.5)	0.70 (0.08)
−45	−45	0.181 (0.005)	−40.1 (0.2)	17.3 (0.5)	3.13 (0.13)
−45	0	0.257 (0.006)	−39.8 (0.1)	18.9 (0.5)	4.86 (0.19)
−45	+45	0.122 (0.005)	−40.0 (0.3)	20.6 (1.0)	2.51 (0.19)
0	−90	0.065 (0.005)	−40.3 (0.4)	17.9 (1.4)	1.17 (0.13)
0	−45	0.221 (0.005)	−40.2 (0.1)	18.9 (0.5)	4.17 (0.14)
0	0	0.352 (0.008)	−39.9 (0.2)	20.1 (0.5)	7.08 (0.29)
0	+45	0.190 (0.005)	−39.9 (0.2)	21.5 (0.6)	4.11 (0.19)
+45	−45	0.095 (0.005)	−41.3 (0.4)	19.3 (1.2)	1.83 (0.16)
+45	0	0.195 (0.006)	−40.4 (0.2)	21.2 (0.7)	4.14 (0.21)
3′ Composite		0.175 (0.003)	−40.2 (0.1)	19.8 (0.4)	3.46 (0.11)

NOTE.—The errors are 1 σ formal errors from the Gaussian fits. For the helium line widths, ΔV_L, systematic effects may make the errors larger than those indicated above.

high velocity wing of the H113β line which would normally appear in the left hand portion of each spectrum.

Table 1 gives the results of the fits for the C90α line. The first column gives the offset of the position in arc seconds from the center of W3 A. The next four columns list the line brightness temperature, velocity centroid, full width at half-maximum, and integrated line strength, respectively. The parentheses enclose 1 σ formal errors for the parameters obtained from the fit to each spectrum. The last column gives the rms dispersion of the residuals along the portion of the spectrum which contained the baseline, the carbon line, and the helium line. Table 2 gives the results of the fits for the He 90α line in

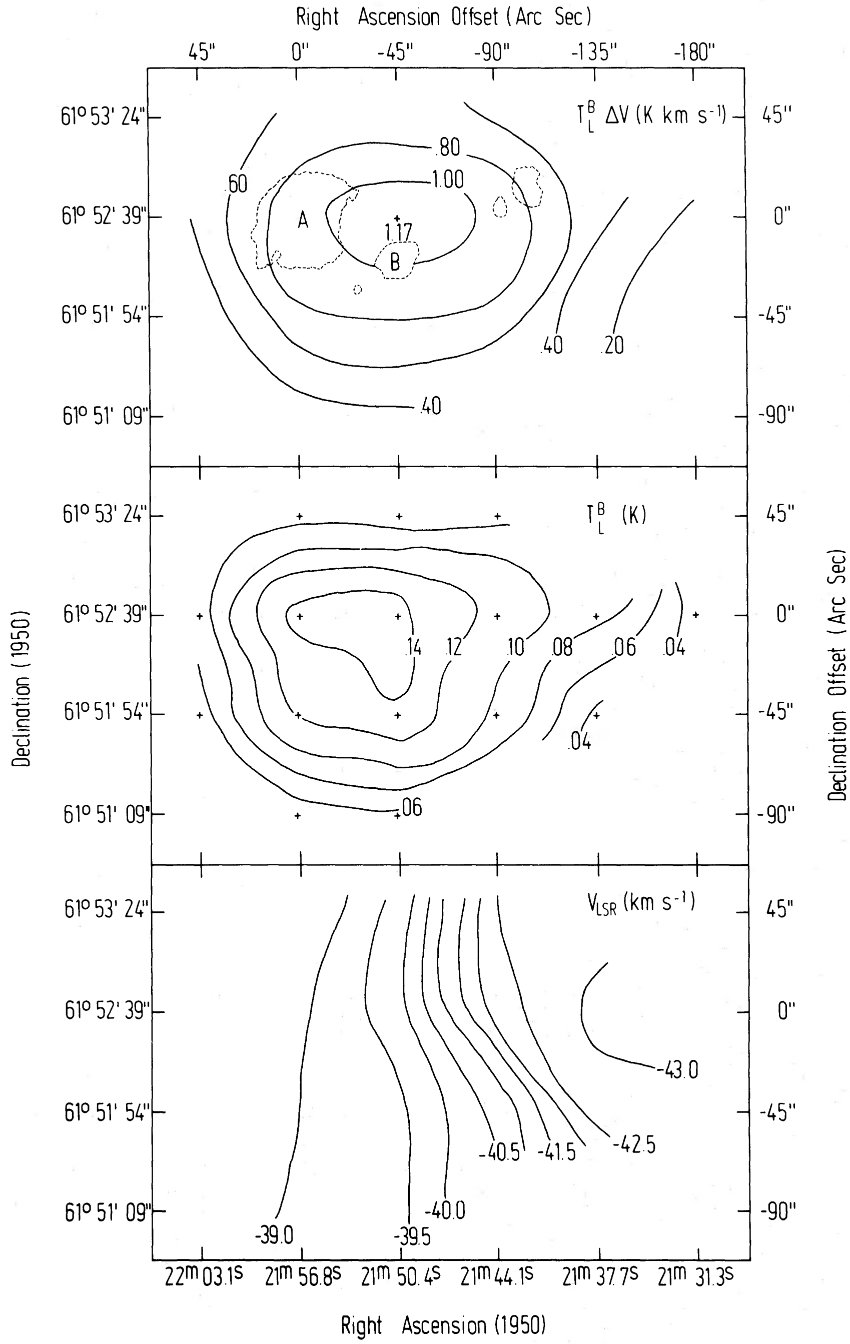

FIG. 2.—(a) (top) The distribution of integrated line strength ($\int T_L^B \Delta V$) as a function of position. The dotted contours are the 255 K continuum level from the map of Harris and Wynn-Williams (1976). (b) ($center$) The T_L^B distribution. The crosses show the points at which the data were taken. (c) ($bottom$) The distribution of LSR velocity of the C90α line across the source.

the same format. The last entry in both tables refers to a spatially averaged composite spectrum which we will discuss in a later section.

Figures 2a–2c display the carbon line parameters in the form of contour maps. The solid lines in Figure 2a are contours of integrated line strength. The dashed contours are the 332 K continuum brightness temperature level taken from Figure 1 of Harris and Wynn-Williams (1976). We follow their designation scheme in labelling the components W3 A and W3 B in Figure 2a. In Figure 2b, the contours show the spatial variation of C90α line brightness temperature. The crosses mark the positions where we took the spectra. Figure 2c shows the spatial variation of radial velocity reduced to the local standard of rest (LSR) using the standard solar motion.

III. MAP OF THE C90α LINE

As shown in Figure 1, we detected the C90α line at all positions included in the map. The weakest line was 4.5 times the formal 1 σ error from the Gaussian fit. We fitted a Gaussian profile to the map of integrated line strengths ($=\int T_L\, d\nu$) to derive the location of the emission peak and the source width. The peak is at $\alpha = 02^h21^m50\overset{s}{.}6 \pm 1\overset{s}{.}3$, $\delta = 61°52'31'' \pm 9''$ (1950.0); west and south of the center of W3 A (W3 IRS 2 [Wynn-Williams, Becklin, and Neugebauer 1972]). The quoted errors combine the 1 σ formal errors from the least-squares fit and the pointing errors assuming that the uncertainties are independent. The peak in a fit of a two-dimensional Gaussian to the peak line temperature distribution (i.e., ignoring the variation in the line width) is $\sim 15''$ east of the peak of the distribution of integrated line strength.

Wilson, Thomasson, and Gardner (1975) mapped the C134α (2.7 GHz) line toward W3 with $4\overset{'}{.}8$ resolution. The half-beamwidth spaced map shows the C134α line at seven positions. The source size, corrected for the beam, was $3' \pm 2'$ where the error is the maximum probable value. Rickard, Zuckerman, and Palmer (1977) attempted to map the C76α line at 14.7 GHz. They detected the line at only one position and obtained an upper limit to the angular size for the region between $1\overset{'}{.}6$ (at the 1 σ level) and $10\overset{'}{.}6$ (at the 3 σ level). Sullivan and Downes (1973) gave a lower limit to the region's size of $0\overset{'}{.}75$ based on their nondetection of the C166α line with the Westerbork synthesis telescope using 20 km s^{-1} wide filters. Virtually all other carbon measurements were made only at the center of the nebula. Our Gaussian fit to the C90α integrated line strength map gives a full width to half-maximum (including our beam) of $151 \pm 13''$ in right ascension and $126 \pm 10''$ in declination. Comparison of this map (Fig. 2a) with the line temperature map (Fig. 2b) indicates good agreement between the source size obtained from the line temperature and integrated line strength distributions. The Gaussian source widths corrected for broadening in a 90$''$ beam are $121'' \pm 17''$ in R.A. and $88'' \pm 15''$ in decl.

The source size measurement permits us to compare our C90α results to earlier results at nearby transitions directly: The corrected integrated line strengths measured at C94α and C92α by Chaisson (1972, 1974) are $\sim$35% lower than the present results. This is within the errors caused by noise, calibration errors, and the uncertainty in the beam efficiency and filling factor corrections.

Examination of Figures 1 and 2c reveals a marked shift in velocity across the carbon source. To the east of the C II peak, the velocity centroid is roughly -39 km s^{-1}; to the west of the peak it is roughly -42 km s^{-1}. All of shift takes place along the north-south axis with $\sim\frac{1}{2}$HPBW. The velocity shift ($\sim$3 km s^{-1}) is considerably larger than the errors in the individual line velocity measurements (typically ± 0.2 km s^{-1}). Dickel *et al.* (1980) and Brackmann and Scoville (1980) have observed a similar shift in the ^{12}CO velocity across this region.

IV. THE -22 km s^{-1} FEATURE

Gordon and Churchwell (1970), observing the C85α line at 10527 MHz, and Chaisson (1971), observing the C94α line at 7797 MHz, have reported, in addition to the main carbon line at -40 km s^{-1}, a second, weaker feature. Because the line appears at the same velocity offset from the -40 km s^{-1} feature at two different

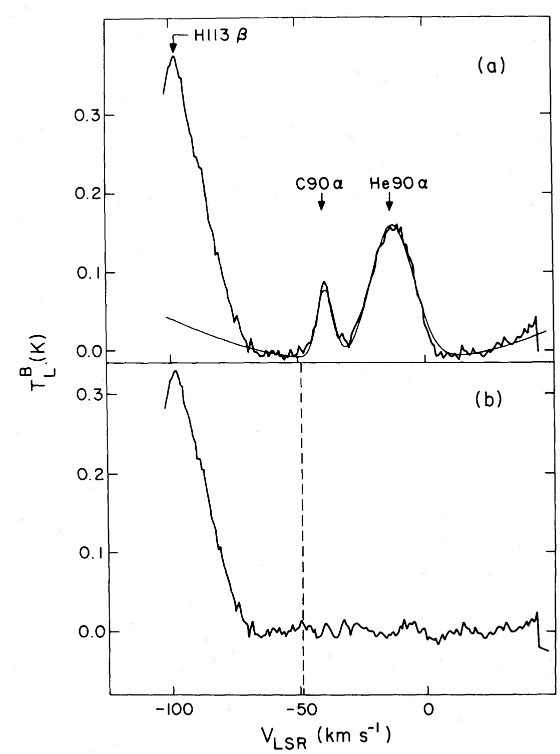

FIG. 3.—The 3$'$ composite spectrum (*top*) and the residuals to a two-Gaussian fit for the helium and carbon lines (*bottom*).

frequencies, it was taken to be a recombination line. If it is due to carbon, the LSR velocity is -22 km s^{-1}. H I, OH, and H_2CO absorption at ~ -20 km s^{-1} lends support to the interpretation of this feature as a carbon line. The feature has not been seen, however, at lower frequencies. Model calculations show that the observed increase in intensity with frequency implies an electron temperature in the C II region of 10^3 K. By averaging our individual spectra with Gaussian weighting, we have synthesized a C90α spectrum with an effective beam size of 3′. This beam is similar to that used in the earlier observations (2′.8 and 4′.4). Figure 3 shows the 3′ C90α spectrum, and the last entries in Tables 1 and 2 give the Gaussian fits for the line parameters. From Table 1 of Chaisson (1971), we obtain a ratio $T_{\mathrm{C\,II}}$ (-40 km s^{-1})/$T_{\mathrm{C\,II}}$ (-22 km s^{-1}) equal to 5.2 ± 2.7. The 3′ beam spectrum made from our data gives a 3 σ lower limit to this ratio of 11.9. That is, our limit shows that the C90α line at -22 km s^{-1} is *at most* only one-half of the temperature reported by Chaisson (1971). The measurement of the -22 km s^{-1} feature reported by Gordon and Churchwell (1970) is ~ 7 times larger than our sensitivity limit. These measurements are therefore inconsistent with our results, and we believe that the previous detections are incorrect.

V. THE HEAVY ELEMENT LINE

We detected no 90α recombination-line emission from elements heavier than carbon (hereafter the Z90α line). The 3 σ lower limit for the ratio of the peak line temperatures, T_L (C90α)/T_L (Z90α) is 10.4. We obtained the limit on the Z90α line by measuring the rms noise in the baseline. The corresponding C/Z$n\alpha$ ratio has been measured at lower frequencies and has a value of 5.8 ± 2.0 at 155α ($\Theta_{\mathrm{Beam}} = 8'.7$), 3.1 ± 0.5 at 158α ($\Theta_{\mathrm{Beam}} = 7'.8$), and 3.4 ± 0.6 at 109α ($\Theta_{\mathrm{Beam}} = 2'.6$; see the collected data of Pankonin *et al.* 1977). Chaisson (1974) reports measurements of the Z92α line with a 4′.2 beam and gives a carbon to heavier element line temperature ratio of 2.1 ± 0.7. The errors are all of these ratios are the 1 σ *formal* errors from the Gaussian fits. This last ratio is inconsistent with our *3σ* lower limit to the line ratio, 12.3, from the 3′ average beam, but the true errors in the noisy 92α spectrum do not exclude the possibility that this result is consistent with our less noisy value. The dashed line in Figure 3 shows where the Z90α line would be, if it were present. Our nondetection of the Z90α line, together with the internally consistent values obtained at low frequencies, indicates that the C and Z emission regions *do not* have the same physical conditions and are therefore not spatially coincident. The changes in the strength of Z$n\alpha$ relative to the C$n\alpha$ line with principal quantum number or beam size imply either (1) that the *z* line region has physical conditions which make the line more subject to stimulated emission at low frequencies, (2) that this region is larger than the carbon region, or (3) a combination of (1) and (2). Because of the change of the measured line temperature ratio with frequency, the Z$n\alpha$/C$n\alpha$ intensity ratio need not reflect the abundance ratio of the emitting ions. This line ratio is therefore an unreliable predictor of elemental depletion in partially ionized gas near H II regions. This has been pointed out previously for the case of heavy element lines in dark clouds (Pankonin and Walmsley 1978).

VI. LINE FORMATION

We can use the C90α map of W3 to address two important questions about line formation in the carbon region: (1) Is the dominant line formation mechanism spontaneous or stimulated emission? (2) What limits can we set on the electron temperature T_e and density N_e?

For a Gaussian shaped beam and C II source, we derive a beam filling factor from the C90α map of 0.57. If the carbon line is emitted from *thin* shells around the compact H II regions or is significantly clumped, the beam filling factor may be smaller, but the ratios of the filling factors for different beam sizes will remain about the same.

We use the C90α measurement, where the beam size is smaller than the source size, to derive the carbon emission measure. For a spontaneously emitting, optically thin region, the emission measure is given by

$$E_{90} = 5 \times 10^4 \frac{T_e^{3/2} \Delta\nu_{90} T_L^B}{f b_{90}} \exp(-195/T_e) \text{ cm}^{-6} \text{ pc}$$

(Dupree and Goldberg 1970) where $\Delta\nu_{90}$ is the C90α line width in kHz, T_L^B the main beam brightness temperature, f the beam filling factor, and b_{90} the non-LTE departure coefficient for $n = 90$. Throughout the discussion, we will use the b_n's of Ungerechts and Walmsley (1979). Table 3 gives the line data for the carbon transitions upon which we base our discussion.

Given the emission measure, we can predict the observed strength of other C$n\alpha$ transitions using an inverted form of equation (1). If the C109α line emission is purely spontaneous, the computed values of T_L^B (C109α) vary from 11% more to 32% less than the observed strength for a range of $N_e = 1-10$ cm^{-3} and $T_e = 10-1000$ K. Thus, it appears that in the spontaneous emission model, the predicted C90α/C109α ratio *can* match the observed ratio within a reasonable range of temperatures and densities. We have used the same method to compare the spontaneous emission model values and the observed values for T_L^B (C158α) observed at 1.6 GHz. Over the same range of temperatures and densities as the C109α comparison, the model C158α line temperatures were never more than 44% of the measured value; that is, the observed C158α line is always stronger than the predicted line. This is a strong

TABLE 3

CARBON LINE DATA

Transition	Ref.[a]	T_L^B (K)	$\Delta\nu$ (kHz)	Filling Factor
C90α	1	0.15 (0.01)	231 (15)	0.57
C109α	2	0.37 (0.03)	87 (7)	0.30
C158α	2	0.68 (0.03)	33 (3)	0.046
C166α	2	0.50 (0.03)	27 (2)	0.038
C199β	2	0.09 (0.02)	33 (6)	0.046

[a]REFERENCES.—(1) This paper. (2) Pankonin *et al.* 1977.

indication that stimulated emission accounts for part of the 158α line intensity.

Pankonin *et al.* (1977) used α/β ratios for pairs of transitions at nearly the same frequency to study the carbon emission. Because they measured the α and β lines at nearby frequencies, the ratios did not depend on beam filling factors. Pankonin *et al.* could not explain the 158α/199β ratio at 1.6 GHz without invoking stimulated enhancement of the C158α line. The observed $T(\text{C}158\alpha)/T(\text{C}199\beta)$ ratio is 7.6, whereas the ratio for optically thin spontaneous emission is less than 3.6. Increasing the postulated optical depth of the C II makes the discrepancy worse. At 5 GHz, stimulated and spontaneous models with similar parameters matched the 109α/137β data equally well. Model calculations show that the observed C109α/C137β ratio does not sensitively determine the extend of stimulated emission because the stimulation has only a small effect on this line ratio compared to the change in the ratio as a function of kinetic temperature and electron density. Earlier investigators also compared the C$n\alpha$ line strengths to models using guesses for the beam filling factor or allowing this quantity to vary as a parameter of the model (see, e.g., Rickard, Zuckerman, and Palmer 1977). These investigations also indicate that stimulated emission must contribute to the line strength of C$n\alpha$ at low frequencies (see, e.g., Dupree 1974), but not at frequencies higher than 5 GHz. The need for stimulated emission to produce the observed C158α line is thus well established, while our observations support a picture in which spontaneous emission dominates the high frequency line formation.

The present observations define the size of the *spontaneously* emitting region, i.e., the C II both in front of and behind the H II region, and show that there is a velocity gradient across the source. Even with these known geometrical and physical properties, any realistic model of the C II region is underconstrained. First, we do not have adequate information about the sizes of the *individual* clouds which are in our 90″ beam; second, we do not know how much of the material at any given velocity is in front of the continuum sources. We therefore cannot determine in detail the characteristics of the various regions. The complexity revealed by our map makes further efforts at using models based on the total C II intensity to obtain electron temperatures and densities a pointless exercise (see Rickard, Zuckerman, and Palmer 1977 for the most recent work using this technique).

VII. SPATIAL VARIATIONS IN V(C90α) AND VARIATIONS IN V(C$n\alpha$) WITH n

As discussed in § III, we see a steep velocity gradient: from roughly -39 km s^{-1} in the east to roughly -42 km s^{-1} in the west. This gradient is especially interesting since Pankonin *et al.* (1977) remarked that there is a trend of increasing radial velocity with increasing frequency. They explain this trend by invoking two positionally coincident C II clouds, one behind W3 A and W3 B with a velocity of -39.2 km s^{-1} and another in front of W3 A and W3 B with a velocity of -40.1 km s^{-1}. At high frequencies, spontaneous emission from the first cloud dominates; at frequencies below 5 GHz, stimulated emission from the second cloud dominates. We find a trend toward lower velocity at larger beam size (for beam sizes less than 9′) which is at least as significant as the variation of $V_{\rm LSR}$ with line frequency. The trend has the appropriate sense for observations made toward the continuum peak: with beams of less than 2′.6 one sees only the part of the cloud at -39 km s^{-1}, while with larger beams one sees a mixture of this part and the -42 km s^{-1} part which lies to the west. Comparing the average velocity weighted by the integrated line strength from our C90α map to the signal-to-noise weighted mean of the C158α, C166α, and C199β velocities of Pankonin *et al.*, we obtain a value of -40.1 km s^{-1} for the C90α data and -40.06 ± 0.09 km s^{-1} for the averaged C158α, C166α, and C199β data. Thus, the previously reported variation of $V_{\rm LSR}$ with frequency may be in fact the result of a variable contribution of the two sides of the cloud which depends on the telescope beam size.

VIII. RELATIONS OF THE C II, H II, AND MOLECULES

Although the C90α map does not help us to determine N_e and T_e in the C II region, the C II velocity and spatial distribution allow us to examine the self-consistency of various ideas about the relation of the

C II region to the compact H II regions and the molecular clouds. The observations show that (1) the C II region lies at the same declination as the H II regions W3 A–D; (2) the distribution of the H II regions is elongated in the east-west direction (as is the C II region and the emission from cool dust (Westbrook *et al.* 1976); and (3) there is a sharp east-west velocity gradient in the neutral (CO, Dickel *et al.* 1980; Brackmann and Scoville 1980), partially ionized (this paper) and ionized gas (see below). Any reasonable picture of the inner part of the W3 complex must take all of these observations into account.

Zuckerman and Palmer (1968) suggested a model for C II regions (in general) in which the C II emission arises in thin shells at the interface between the ionized gas and the dense neutral cloud. The dynamics of the Orion A C II region (Jaffe and Pankonin 1978) lend support to this model. In the case of W3, however, we have not resolved an individual region but must look at several compact H II region/molecular cloud boundaries in each telescope beam. The coincidence of the C II region with the H II regions W3 A–D argues that the C II and H II regions are associated but does not help to distinguish between a picture in which the C II emission comes from dense shells around the H II regions and one in which this emission arises in a uniform, diffuse source which encompasses the entire H II region complex. Together with the observation that the C II region is elongated and has the same extent as the group of H II regions, however, the positional coincidence strengthens the case for the shell picture. We argue in § VI that the C90α emission is primarily spontaneous. A spontaneously emitting diffuse region or a region in a large ionization front associated with the more broadly distributed molecular material in this region (Lada *et al.* 1978) would not necessarily coincide with the compact H II regions. This is especially true since most of the H II regions seem to be strongly ionization-bounded (Harris and Wynn-Williams, 1976). One would expect C II–emitting shell sources, however, to coincide with the compact H II regions and to peak at a position where the telescope beam covered a maximum amount of shell surface area. This is precisely what the observations show.

The observation of a velocity gradient (point [3] above) argues strongly for the dense shell picture. Harris and Wynn-Williams (1976) have found that 75–100% of the radio continuum emission in W3 comes from the compact sources. The helium recombination line, which originates in the same gas as the continuum emission, is therefore a reliable probe of the dynamics of the compact sources. We took the helium and carbon data simultaneously. We can therefore compare them directly in order to study the relative velocity of the ionized and partially ionized gas. Table 4 lists the intensity-weighted mean helium and carbon line velocities for the eastern and western portions of the nebula. The first column contains the average of all positions east of and including ΔR.A. $= -45''$. We have excluded the position ΔR.A. $= 90''$, Δdecl. $= -45''$, from the averages since the velocity at this position is halfway between the velocities of the two components. The average velocity for the western component is less certain than that for the eastern component because of both poorer signal-to-noise ratios for the lines and larger point-to-point variations in the line velocities. Table 4 indicates that both the helium and carbon line velocities are 3–4 km s^{-1} higher in the east than in the west. This similarity in the variation of the radial velocity of C II and He II indicates strongly that the ionized and partially ionized regions are close together and share whatever systematic motion is present in the core of the W3 region.

TABLE 4

MEAN VELOCITIES

Transition	$\alpha \geq -45''$	$\alpha < -45''$
He 90α......	-40.2 km s^{-1}	-44.5 km s^{-1}
C90α	-39.1 km s^{-1}	-42.6 km s^{-1}

It is interesting in terms of both the location of the partially ionized region and the structure of the molecular cloud, to compare the observed C II velocity pattern with the velocity pattern in H_2CO and ^{12}CO and ^{13}CO (Bieging, Downes, and Wilson 1981; Dickel *et al.* 1980; Brackmann and Scoville 1980). All three of these molecules show a change in velocity from -38 km s^{-1}, 1′ southeast of W3 (IRS 5) (near the C II peak) to -43 km s^{-1} 1′ northwest of this point. Brackmann and Scoville (1980) have argued that this velocity shift represents rotation of the molecular cloud core. The ^{12}CO temperature and ^{13}CO and H_2CO column density all peak toward the compact continuum sources. This observation argues that the molecules are close to these sources and that the ^{12}CO is heated by them. If the rotation picture is correct, the massive neutral component of the cloud core must dominate the dynamics. The embedded ionized and partially ionized regions are then carried along at the local velocity of the neutral region in which they are embedded.

A part of this work was done while T.L.W. was a guest at the Radio Astronomy Laboratory, University of California, Berkeley, where research is supported in part by NSF grant AST78-21037.

REFERENCES

Bieging, J., Downes, D., and Wilson, T. L. 1981, in preparation.
Brackmann, E., and Scoville, N. Z. 1980, *Ap. J.*, **242**, 112.
Chaisson, E. J. 1971, *Ap. J. (Letters)*, **167**, L61.
______. 1974, *Ap. J.*, **191**, 411.
Dickel, H. R., Dickel, J. R., Wilson, W. J., and Werner, M. W. 1980, *Ap. J.*, **237**, 711.
Dupree, A. K., and Goldberg, L. 1970, *Ann. Rev. Astr. Ap.*, **8**, 239.
Gordon, M. A., and Churchwell, E. B. 1970, *Astr. Ap.*, **9**, 307.

Harris, S., and Wynn-Williams, C. G. 1976, *M.N.R.A.S.*, **174**, 649.
Jaffe, D. T., and Pankonin, V. L. 1978, *Ap. J.*, **226**, 869.
Lada, C. J., Elmegreen, B. G., Cong, H. I., and Thaddeus, P. 1978, *Ap. J. (Letters)*, **226**, L39.
Mezger, P. G., and Wink, J. E. 1975, in H II *Regions and Related Topics*, ed. Wilson and Downes (Berlin: Springer), p. 408.
Ogura, K., and Ishida, K. 1976, *Pub. Astr. Soc. Japan*, **28**, 651.
Pankonin, V. L., and Walmsley, C. M. 1978, *Astr. Ap.*, **64**, 333.
Pankonin, V., Walmsley, C. M., Wilson, T. L., and Thomasson, P. 1977, *Astr. Ap.*, **57**, 341.
Reifenstein, E. C., Wilson, T. L., Burke, B. F., Mezger, P. G., and Altenhoff, W. J. 1970, *Astr. Ap.*, **4**, 377.
Rickard, L. J., Zuckerman, B., and Palmer, P. 1977, *Ap. J.*, **218**, 659.
Sullivan, W. T., and Downes, D. 1973, *Astr. Ap.*, **29**, 369.
Ungerechts, H., and Walmsley, C. M. 1979, *Astr. Ap.*, **80**, 325.
Westbrook, W. E., Werner, M. W., Elias, J. H., Gezari, D. Y., Hauser, M. G., Lo, K. Y., and Neugebauer, G. 1976, *Ap. J.*, **209**, 94.
Wilson, T. L., Thomasson, P., and Gardner, F. F. 1975, *Astr. Ap.*, **73**, 167.
Wynn-Williams, C. G., Becklin, E. E., and Neugebauer, G. 1972, *M.N.R.A.S.*, **160**, 1.
Zuckerman, B., and Palmer, P. 1968, *Ap. J. (Letters)*, **153**, L145.

D. T. Jaffe: Enrico Fermi Institute, University of Chicago, 5630 S. Ellis Avenue, Chicago, IL 60637

T. L. Wilson: Max-Planck-Institut für Radioastronomie, Auf dem Hügel 69, 5300 Bonn, Federal Republic of Germany